


Polarization Transfer from Optically Pumped Ensembles of N-V Centers to Multinuclear Spin Baths

R. Rizzato,¹ F. Bruckmaier,¹ K.S. Liu,¹ S.J. Glaser^{1,2,*} and D.B. Bucher^{1,2,*}

¹*Department of Chemistry, Technical University of Munich, Lichtenbergstraße 4, Garching bei München 85748, Germany*

²*Munich Center for Quantum Science and Technology (MCQST), Schellingstr. 4, München D-80799, Germany*

 (Received 18 July 2021; revised 25 November 2021; accepted 7 January 2022; published 24 February 2022)

Nitrogen-vacancy (N-V) diamonds have attracted keen interest for nanoscale sensing and spin manipulation. In particular, the nonequilibrium electron spin polarization after optical excitation of single N-V centers has successfully been transferred to nuclear spin baths in the surrounding of defects. However, these experiments need to be extended to N-V ensembles that have promising practical applications in the hyperpolarization of bulk sample volumes for NMR signal enhancement. Here, we use a dense, shallow ensemble of N-V centers to demonstrate polarization transfer to nuclear spins in a well-defined composite diamond sample system. This allows us to address three different types of nuclear spins in different positions with respect to the N-V polarization source: from the close proximity of ¹³C inside the diamond lattice to the self-assembled molecular system consisting of ¹H and ¹⁹F spins outside the diamond and over multiple interfaces. We show that ensemble N-V experiments face problems different from single N-V experiments. In particular, using spinlock pulses, the inhomogeneously broadened electron spin resonance line of the N-V ensemble limits the minimal resonance linewidth with which the transfer protocol can occur. Furthermore, we compare the N-V spin-polarization losses and polarization transfer rates to the different nuclear baths and discuss the role of spin diffusion as detrimentally affecting the direct observation of nuclear polarization buildup within the detection volume of nanoscale N-V-NMR experiments.

DOI: [10.1103/PhysRevApplied.17.024067](https://doi.org/10.1103/PhysRevApplied.17.024067)

I. INTRODUCTION

Nuclear magnetic resonance (NMR) encompasses a wide range of techniques that are of fundamental importance for the chemical characterization of organic and inorganic materials as well as of biological and complex systems. However, NMR spectroscopy lacks sensitivity, due to the extremely low nuclear spin polarization that generates the detected signal. To overcome the issue, hyperpolarization methods, such as dynamic nuclear polarization (DNP), have emerged consisting of well-suited microwave (MW) irradiation schemes that allow us to transfer the higher thermal polarization of the electron spins to the target nuclei [1–4]. In contrast, the electronic spin of the nitrogen-vacancy (N-V) center in diamond can be highly polarized by optical excitation at room temperature and coherently manipulated, forming a promising hyperpolarization platform [5–8]. Although direct detection of spin-polarization buildup has not been demonstrated yet for nuclei external to the diamond, the polarization transfer from N-V centers to nuclear spins has

been accomplished either within the (nano)diamond lattice [9–13] or from single N-V centers to small external nuclear ensembles [14–16]. However, the latter systems are limited to the nanoscale and are not suited for applications in micronscale N-V-NMR experiments [17–20], bulk NMR, or biomedical imaging, where the ratio between the number of N-V defects and target nuclei needs to be significant. Scaling up the N-V system by means of ensembles is then necessary, but not trivial since they face different problems due to their density and spatial distribution. Inhomogeneous properties throughout the ensemble, shorter coherence times, and inhomogeneities of both the driving MW field and the static magnetic field are only examples of the issues that need to be tackled when working with N-V ensembles and that are to be investigated in detail.

Here, we report on the use of shallow-implanted N-V ensembles for the direct transfer of optically pumped electron spin polarization to nuclear spins internal to the diamond lattice and external to a well-defined self assembled monolayer [21]. Such a system has been chosen since it has several advantages: (1) it is a well-defined solid-state sample with known surface chemistry, (2) it contains several types of NMR active nuclei that can be addressed

*dominik.bucher@tum.de

at the same time, (3) it permits the exploration of spin-polarization transfer over multiple interfaces, and (4) its thin structure of 2–3 nm allows us to exploit a certain degree of confinement for external nuclear polarization accumulation and storage.

The polarization transfer is accomplished through an experiment known as nuclear spin orientation via electron spin locking (NOVEL) that belongs to the family of NMR signal enhancement techniques, more specifically, pulsed DNP experiments [22–24]. Here, the electronic spin of the N- V defect in diamond is brought into a superposition state by a strong $\pi/2$ pulse and then locked on the transversal plane of the laboratory frame by a long spinlock pulse of variable amplitude. In this manner, an electron spin dressed state is created and preserved for a time interval of the order of its rotating frame spin-lattice relaxation time $T_{1\rho}$, namely a few hundreds of microseconds. During this time, the electronic dressed state can be brought in energy contact with the nuclear spin by matching the MW field strength used to lock (or “dress”) the electronic spin with the Larmor frequency of the target nuclear spins ($\nu_{\text{IN-}V} = \nu_{0n}$). This is the so-called *Hartmann-Hahn* (HH) matching condition [25], well known in NMR when cross-polarization experiments between different nuclear spins are performed, but also utilized in some of its variants in the fields of electron spin resonance (ESR) and DNP, to accomplish polarization transfers between electron and nuclear spins [24,26–28].

In order to probe the actual polarization of the nuclear target, we compare the effects observed with the NOVEL experiment with those resulting from the polarization read-out via polarization inversion (PROPI) experiment [13,24,29]. In PROPI, two NOVEL pulse sequences are applied one after the other, differing only in the spinlock pulse phase that is set to polarize the nuclear spins in two opposite directions. Then, if the first block of the sequence polarizes the nuclear spins in the “up” state, the second polarizes in the “down” state or vice versa. In this manner, it is possible to probe the extent to which the nuclear ensemble has been effectively polarized and preserves the polarization throughout the experimental timescale. We explore the efficiency of the spinlock pulse sequence and its potential to build-up nuclear polarization by cycling the experiment in a competition with nuclear relaxation and spin diffusion processes.

II. METHODS

A. Diamond properties and sample preparation

All experiments are based on a $2 \times 2 \times 0.5$ mm³ electronic grade diamond [natural (1.1%) ¹³C abundance, Element Six] that is implanted using ¹⁵N at an energy of 2.5 keV with a fluence of 2×10^{12} /cm² (Innovion) and subsequently annealed [30]. This results in a distribution of near-surface N- V centers about 5 nm below the

surface. For these implant conditions, a N- V density of about 50–100 N- V centers per square micrometer can be estimated [31,32]. The T_1 and T_2 of our shallow N- V ensemble are about 650 and 4 μ s, respectively. Before performing experiments on clean diamond as well as before every Al₂O₃ deposition, the diamond is cleaned with a protocol involving equal parts of boiling sulfuric, nitric, and perchloric acid (triacid cleaning) according to Brown *et al.* [33]. For the preparation of the system, atomic layer deposition (ALD) is performed for the deposition of a 1-nm-thick Al₂O₃ film, followed by phosphonic acid surface functionalization and formation of monolayer as described in detail in Liu *et al.* [21]. The number of spins considered throughout the work for the ¹⁹F ensemble (around 3000 for a single N- V center) has been estimated from the work of Liu *et al.* for a similar system.

B. Experimental setup

The experiment is based on a modified version of the setup described in Bucher *et al.* [30]. The diamond chip is positioned between two permanent magnets, which are rotated and tilted such that the B_0 field is aligned with one of the four possible N- V center orientations. The distance of the magnets is adjusted in order to reach the working magnetic field strength B_0 (in this work about 88 mT). Initialization of the N- V ensemble is achieved by using a 532 nm laser (Opus 532, Laser Quantum) at a power of around 200 mW at the diamond position. The laser light is focused on the diamond by a planoconvex lens (LA1986-A-M, Thorlabs) in a total internal reflection geometry. The laser pulses are controlled by an acousto-optic modulator (model 3260-220, Gooch and Housego) with pulse durations of 5 μ s. For quantum control of the N- V centers, microwave pulses are directly synthesized with an arbitrary waveform generator (AWG5202, Tektronix), allowing precise control of the phase and frequency, then amplified using a microwave amplifier (ZHL-100W-52 S+, Mini-Circuits). A homebuilt microwave loop is utilized to deliver microwave to the sample. The diamond is glued to a thin glass cover slide (48393-026, VWR) and a 6 mm glass hemisphere (TECHSPEC[®] N-BK7 Half-Ball Lenses, Edmund Optics) is glued to the other side, in order to improve the light collection. This assembly is then glued to a 30 mm cage plate (CP4S, Thorlabs) and mounted above two condenser lenses (ACL25416U-B, Thorlabs) that collect and collimate photoluminescence (PL) to an avalanche photodiode (A-CUBE-S3000-03, Laser Components GmbH). A long-pass filter (Edge Basic 647 Long Wave Pass, Semrock) placed between the last condenser lens and the photodiode is used to remove the excitation wavelength from the PL light. The photovoltage is digitized with a data acquisition unit (USB-6281 DAQ, National Instruments). A homebuilt wire coil placed above the diamond delivered the reference

rf signals that are synthesized by an arbitrary waveform generator (DG1022Z, RIGOL).

III. RESULTS

A. Characterization of the spinlock experiment with N-V ensembles

Before performing the actual experiments on nuclear spin samples, it is useful to characterize the pulse sequence by means of an external radiowave frequency (rf) field in the megahertz range that mimics the oscillating magnetic fields generated by nuclear spin precession. Since such an experiment does not rely on actual polarization transfer to nuclear spins, we distinguish it from NOVEL by simply calling it the “spinlock” experiment. For this purpose, a rf coil is mounted a few millimeters above the diamond chip in the experimental setup. The coil is oriented such as to generate an oscillating magnetic field parallel to the orientation of the external B_0 field. The spinlock pulse sequence is set up as shown in Fig. 1(a). Driving the N-V ensemble at the resonance frequency and sweeping the spinlock field

amplitude while continuously irradiating at a certain radio frequency results in a fluorescence contrast dip as soon the N-V Rabi frequency matches the frequency of the applied rf field. This can be described by considering the N-V spins to be in a dressed state basis, where the new quantization axis lies in the x - y plane of the laboratory frame. Matching the energy splitting by means of an oscillating field along the z axis can induce transitions between the dressed “plus” state and the “minus” state (or vice versa), leading to a reduction in fluorescence [see Fig. 1(b)]. In Fig. 1(d) the experiment is shown for rf reference signals with different frequencies. From this, it is possible to build a calibration curve of the applied rf frequency versus the spinlock MW amplitude as shown in Fig. 8 in Appendix B. In contrast to single N-V experiments, the depolarization dips show a characteristic lineshape that is tailed toward lower MW amplitudes and becomes overall sharper when higher reference frequencies are matched. Such a behavior can be explained by the fact that, during the experiment, the rf field is set at a constant frequency and is matched with the Rabi frequencies of the N-V

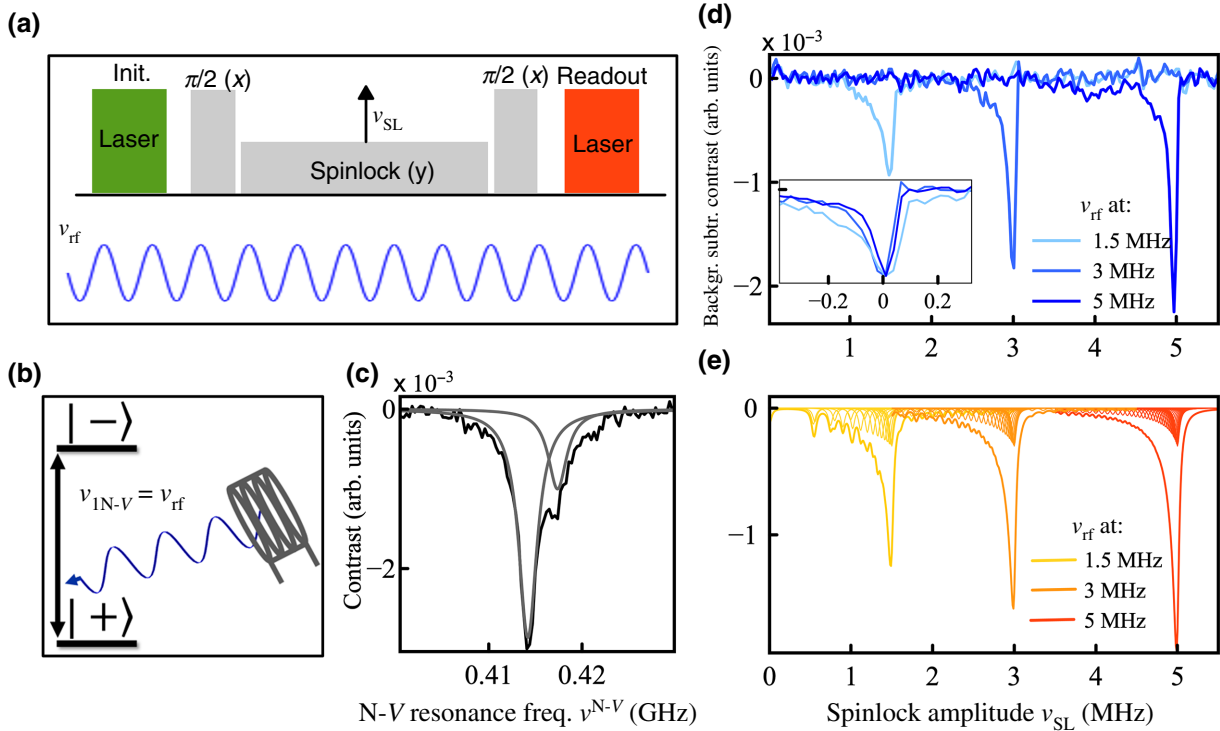


FIG. 1. Spinlock experiment, calibration, and characterization of the pulse sequence for a N-V ensemble. (a) Spinlock pulse sequence. First, a short laser pulse is applied to optically polarize the N-V ensemble into the $m_s=0$ state. Then a MW pulse sequence consisting of $(\pi/2)_X$ -spinlock $_Y$ - $(\pi/2)_X$ pulses is applied. The final spin state is read out by fluorescence with a photodiode. Throughout these events, an oscillating magnetic field with frequency ν_{rf} in the megahertz range is continuously applied with a wire loop (blue). (b) Schematic of the experiment with matched radio frequency. Transitions between electronic dressed states are driven when a coil generates a rf field that matches the splitting. (c) ESR spectrum of the N-V ensemble corresponding to excitation of the N-V transition from the $m_s = 0$ to the -1 state. The spectrum is split by the ^{15}N spin of the N-V center and fit with two Lorentzian functions. (d) Calibration of the spinlock’s amplitude. The rf is kept at a fixed frequency and the spinlock pulse’s amplitude is swept. N-V depolarization appears as asymmetric dips in the optical contrast as soon as the MW field strength matches the rf. Inset: the three dips are overlaid for a linewidth comparison. (e) Simulated depolarization dips (see Appendix A for details).

ensemble: $\nu_{\text{rf}} = \nu_{1\text{N-V}}$. Distinct from the single N- V case, in a dense ensemble, the ESR resonance line [reported in Fig. 1(c)] is inhomogeneously broadened, leading to a linewidth of about 2.4 MHz in our case. Although we can assume a full excitation of the ensemble since the MW excitation bandwidth covers the entire ESR spectrum (as the former in our case is around 10 times larger), the various “spin packets” (homogeneously broadened components of the spectrum; see Appendix A and Fig. 7 therein) will resonate at frequencies $\nu_i^{\text{N-V}}$ slightly different from the N- V resonance frequency $\nu_0^{\text{N-V}}$ at which we tune our MW (normally the center of the ESR line). Thus, although with different contributions, they will all take part in the spinlock process, but the N- V Rabi frequency $\nu_{1\text{N-V}}$ will rather be a distribution of “effective” driving fields, such as $\nu_{1\text{N-V},i} = \sqrt{\Omega_i^2 + \nu_{\text{SL}}^2}$, where $\Omega_i = \nu_0^{\text{N-V}} - \nu_i^{\text{N-V}}$ is the offset frequency for the i th spin packet (or detuning) and ν_{SL} the MW amplitude of the spinlock pulse. For instance, for the 0th spin packet at *exact resonance*, $|\Omega_0| = 0$ and the N- V Rabi frequency would purely correspond to the spinlock amplitude that is matched to the rf: $\nu_{1\text{N-V},0} = \nu_{\text{SL}} = \nu_{\text{rf}}$. Whereas, for off-resonant N- V spin packets, $|\Omega_i| \neq 0$ and this causes the Rabi frequency to be shifted from the spinlock amplitude that can no longer satisfy the matching condition, being $\nu_{1\text{N-V},i} > \nu_{\text{SL}} = \nu_{\text{rf}}$. Thus, since ν_{rf} is kept constant, a smaller value of ν_{SL} will be required to match the condition with $\nu_{1\text{N-V},i}$ and these off-resonant N- V centers will all contribute to provide the observed asymmetry, as also described in Appendix A. Moreover, the dip becomes sharper at high frequencies since the off-resonant contributions become less and less important with respect to the driving field ν_{SL} applied. Simulation of such features have been reported in Fig. 1(e) and have been computed considering the contributions to the depolarization line-shape arising from the off-resonant spin packets of the N- V ensembles within the ESR spectral linewidth, as detailed in Appendix A. As we will see later, such spectral features are preserved during the NOVEL and PROPI experiments on actual nuclear spins. As a result, we conclude that higher matching frequencies are preferable using N- V ensembles. Another effect influencing the depolarization dip linewidth and the overall performance of the spinlock experiments arises from the inhomogeneity of the driving MW field over the N- V ensemble (see Appendix B).

B. A composite multinuclear system for polarization transfer

As a model system, the surface of a diamond chip previously implanted with about 5 nm deep N- V centers is functionalized with a 1 nm layer of Al_2O_3 prepared by ALD. On such a thin film, a self assembled monolayer (SAM) of polyfluorinated organic molecules is grown [21] (see Fig. 2). With this system we can address three types of nuclear spins that are in very different conditions with

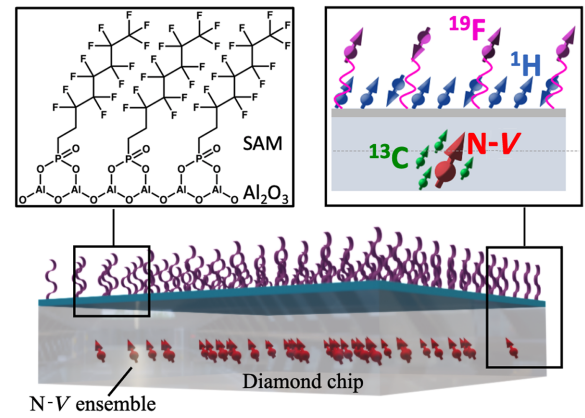


FIG. 2. A composite multinuclear system for polarization transfer. Schematic of the probed diamond system. A chip containing ensembles of near-surface N- V centers is ALD coated with a thin (1 nm) film of Al_2O_3 modified with a monolayer of 1H, 1H, 2H, 2H-perfluoroctanephosphonic acid molecules. The N- V ensemble is used to transfer spin polarization to the nearby ^{13}C spins and to ^1H and ^{19}F spins outside of the diamond lattice.

respect to their interaction with the N- V ensembles: (i) ^{13}C nuclei in natural abundance are located inside the diamond lattice, in close proximity to the N- V centers and interact strongly; (ii) ^1H spins are known to be ubiquitous at the diamond surface [34], though their properties (density, spatial distribution and location, mobility, physical state, etc.) are unknown; (iii) ^{19}F nuclei are bound to the molecules constituting the SAM, and their spin has a natural abundance of 100% and a gyromagnetic ratio comparable to that of protons, but unlike from ^1H , they can be unambiguously assigned to our well-defined surface [21]. It is important to keep in mind that our N- V ensemble is a rather diluted system, where we estimate an average distance between N- V centers of about 100 nm [31,32]. Every N- V center can be then considered as an independent spin system throughout the sample space dictated by our laser spot size (around $4000 \mu\text{m}^2$). For this reason, all effects observed throughout this work will be referred to as a system composed of a single N- V center and an ensemble of nuclear spins.

C. Polarization transfer to nuclear spins

As schematically depicted in Fig. 3(a), during a NOVEL experiment, the N- V dressed states are split by their Rabi frequency $\nu_{1\text{N-V}}$ and can be brought in energy contact with the nuclear bare states by matching the MW amplitude with the nuclear Larmor frequency. Such a protocol can be repeated many times, since the N- V spin can be reinitialized in the $m_s = 0$ state by laser excitation each time. In each of these repetitions, spin-polarization transfer can occur and a consequent drop in the N- V spin signal is detected as a decrease in PL (depolarization dips). However, if during a NOVEL experiment the interacting

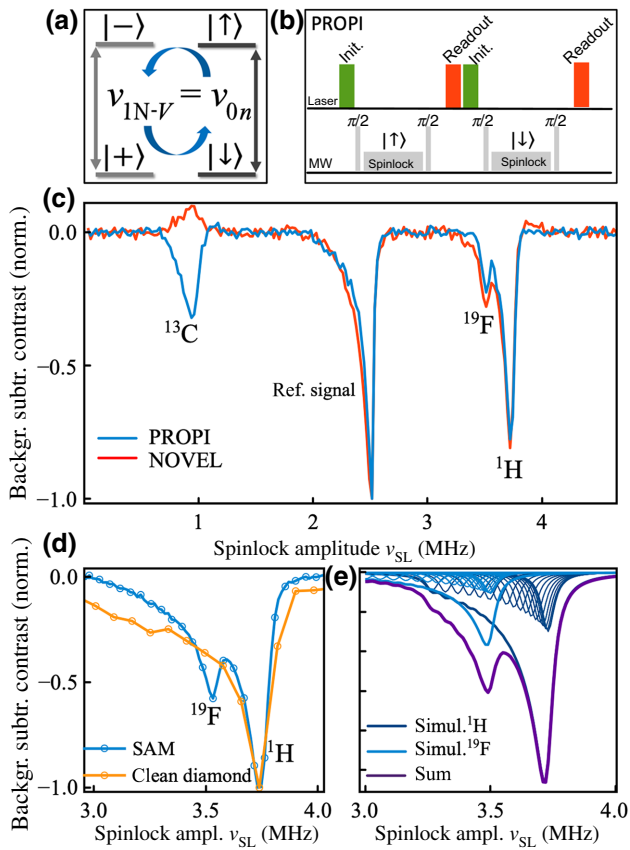


FIG. 3. Nuclear spin detection by the matched Hartmann-Hahn condition with a $N-V$ ensemble. (a) Schematic of the energy matching mechanism between electron spin dressed states and nuclear spin bare state. (b) PROPI pulse sequence. (c) PROPI versus NOVEL experiment. Matched HH condition corresponding to ^{13}C , ^{19}F , and ^1H resonances results in a depolarization of the $N-V$ spin states and consequent dips in the PL contrast for PROPI (blue line), whereas the ^{13}C dip disappears in the NOVEL experiment (red line). A dip from a reference signal of 2.5 MHz frequency is also shown. (d) Detailed PROPI depolarization spectrum around the ^{19}F and ^1H Larmor frequencies. The line in yellow shows the same spectrum for a cleaned diamond without surface modification. (e) Simulated lineshape; see details in Appendix A.

nuclear bath becomes completely polarized, a “saturation” of the system would cause the depolarization dips to no longer be observable. In a PROPI experiment [Fig. 3(b)], two NOVEL sequences are run consecutively, differing only in the phase of the spinlock pulses that is shifted by π with respect to each other [28]. In this manner, the second spinlock pulse neutralizes the nuclear polarization generated by the first one, allowing the dips to always be observable, independently of the nuclear spin bath’s polarization level. A comparison of the NOVEL (red line) versus PROPI (blue line) is shown for our composite multinuclear system. The amplitude of a 40 μs spinlock pulse is swept in a range corresponding to Larmor

frequencies of the probed nuclear spin types at a magnetic field B_0 of 88 mT. The PROPI sequence reveals four intense depolarization dips, where the signal at 2.5 MHz corresponds to a rf reference signal and the dips around 0.94, 3.55, and 3.73 MHz correspond to matching with the Larmor frequencies of ^{13}C , ^{19}F , and ^1H nuclei, respectively [Fig. 3(c), blue line]. Because of the similar gyromagnetic ratios of ^{19}F and ^1H , the Larmor frequencies differ by less than 200 kHz and the signals are partially overlapped. Nevertheless, as shown in Fig. 3(d), they can be clearly distinguished. A different outcome is reported when using the NOVEL pulse sequence [Fig. 3(c), red line]. In this case, the ^{13}C dip disappears and even undergoes an inversion, whereas all the other peaks, including the reference one at 2.5 MHz, preserve their lineshapes and amplitudes. The experimental conditions for both experiments are kept the same, with each spectral point being the result of 5000 repetitions of the pulse sequence (around 100 μs long) and 20 averages of the full amplitude sweep for an experimental time of around 100 s per sweep. The signal is then computed as the difference between the two consecutive optical readouts [Fig. 3(b)] divided by their sum and then normalized to the intensity of the reference signal. Note that peaks at higher frequencies are narrower and that NOVEL and PROPI experiments result in the same lineshapes as in the reference spinlock experiments described in Fig. 1(e). Simulations showing the effect of the off-resonant $N-V$ defects to the overall lineshape are performed and reported in Fig. 3(e). Finally, the same experiments are performed on a clean diamond upon removal of the SAM and Al_2O_3 layer by means of an acid treatment [Fig. 3(d), yellow line]. As expected, the ^{19}F signal is now absent and only signals due to ^{13}C and ^1H matching (see the full sweep spectrum in Appendix B).

D. Study of the polarization transfer dynamics

In the next step we extract dynamic information about the transfer process, by monitoring the fluorescence contrast while increasing the spinlock pulse duration (Fig. 4). As the spinlock pulse gets longer, the detected signal evolves in an exponential decay that is mainly determined by two simultaneous processes. First, electron spin relaxation will manifest with a rotation-frame characteristic time $T_{1\rho}$. This parameter can be easily measured by setting the spinlock amplitude such that the HH condition is not satisfied. This corresponds to the “unmatched HH” curves in Figs. 4(a), 4(c), and 4(e) whose fittings give $T_{1\rho}$ time constants of about 109 μs for ^{13}C , and about 225 μs for ^{19}F and ^1H . In the second case, at the HH condition, enhanced signal loss is caused by additional matching with the nuclear spin bath, i.e., polarization loss to the spin baths [see Figs. 4(a), 4(c), and 4(e)]. We assume that, for each spinlock duration used in the experiment, such an excess of depolarization observed in the matched

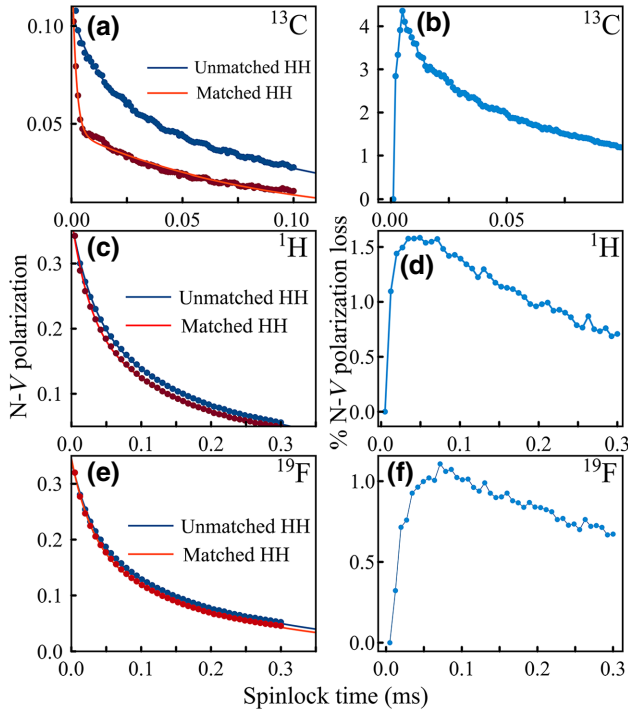


FIG. 4. Polarization transfer dynamics. N- V spin polarization during the PROPI experiment is monitored while varying the spinlock time in the cases of the matched (red dots) and unmatched (blue dots) HH conditions for ^{13}C (a), ^1H (c), and ^{19}F (e). By subtracting the matched and unmatched data points, respective difference curves in (b), (d), and (f) are obtained, showing the percentage of N- V spin depolarization due to polarization transfer. The decays are fit with a biexponential function, as reported in Appendix B.

case versus the unmatched one is due to spin-polarization transfer to the nuclear target. Thus, the contribution due to relaxation mechanisms can be distinguished from the polarization transfer by simply subtracting the two curves [8] [Figs. 4(b), 4(d), and 4(f)]. The maximum of such difference curves then corresponds to an experimental depolarization of the N- V spin of around 4.5% after 5 μs spinlock for ^{13}C , 1.5% after 40 μs for ^1H , and 1% after 65 μs for ^{19}F .

IV. DISCUSSION

Our observations show that spin polarization of the N- V ensemble undergoes significant losses upon application of spinlock-based pulsed schemes at the HH matching condition. A polarization transfer to all three nuclear species addressed in this work can thus be anticipated. In particular, transfer to ^{13}C spins inside the diamond is expected to be an efficient process due to the close proximity of the nuclei to the N- V centers and the consequent strong couplings (up to hundreds of megahertz) that leads to transfer rates several orders of magnitude faster than nuclear

spin relaxation rates [35–38]. The depolarization dip in Fig. 3(c) indeed becomes fully suppressed by the NOVEL experiment, indicating that total polarization of the target nuclear ensemble has been achieved. Moreover, an inversion of the detected contrast is observed. This is possible since, after a certain number of pulse sequence repetitions, the $T_{1\rho}$ relaxation acting during the spinlock causes the N- V spin polarization to decay at a polarization level that is lower than what the ^{13}C polarization buildup has been able to reach. Thus, a polarization transfer from the nuclear ensemble back to the N- V ensemble can occur, as described in more detail in Appendix C and Fig. 12. In the experiments shown in Figs. 4(a) and 4(b), the depolarization of the N- V spin reaches about 4.5% after a 5 μs spinlock time. Thus, assuming that an interacting ^{13}C spin bath would symmetrically gain spin polarization and that it will be shared by all nuclear spins in the ensemble (proportionally to their coupling to the N- V center), a polarization of 4.5%/N is expected for the whole bath, where N is the number of nuclei. This would result in a rate constant for the polarization transfer from the N- V centers to the nuclear spins of $k_{\text{SI}} = 9000 \text{ s}^{-1}$, resulting in a timescale of the order of 2–3 ms to polarize a few ^{13}C nuclei in the close surrounding of a N- V center. On the contrary, in the case of nuclei more distant from the N- V centers, such as ^1H and ^{19}F spins outside the diamond, the weaker interactions determine much slower rates, as shown in Figs. 4(c) and 4(e). Moreover, longer times would be needed for a complete polarization of these ensembles, since the number of spins is higher compared to the ^{13}C bath. The effective polarization transfer rates measured in the experiments in Figs. 4(d) and 4(f) amount to 375 and 154 s^{-1} for ^1H and ^{19}F , respectively. This means for instance that build-up times of the order of several seconds for an ensemble of a few thousand spins are expected (about 3000 ^{19}F spins are estimated to be present in our monolayer in the proximity of a N- V center). It is worth noting that our simulations consider an ideal N- V spin polarization of 100%. However, as reported in Fig. 4, the actual polarization available for the transfer during our experiments is only a fraction of it, i.e., about 10% for the experiments on ^{13}C and 30% for the ^1H and ^{19}F matchings. Thus, the maximum nuclear polarization achievable in these conditions scales accordingly. Such a behavior is likely due to the low MW amplitude of the driving field that causes inefficient spin locking and consequent fast N- V $T_{1\rho}$ relaxation. Such an issue motivates work at higher fields where the matching fields will be proportionally higher in amplitude, resulting in more efficient spinlock pulses. Nevertheless, considering that these dynamics occur on the same timescale as the nuclear spin-lattice relaxation T_{1n} , nuclear polarization buildup is still expected to be observable, at least to some extent. However, no effect has been observed in the NOVEL experiments described above for such

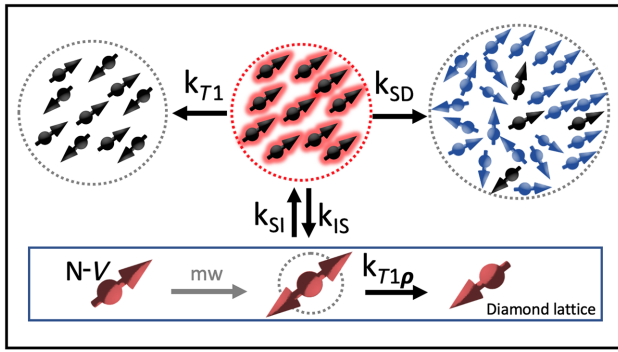


FIG. 5. Simplified rate equation model for polarization buildup. Schematic representation of a N-V ensemble brought in thermal contact with a bath of target nuclear spins. The rate constants of polarization exchange between N-V and nuclear ensembles are represented by $k_{SI} = k_{IS}$, that for polarization loss by spin diffusion to other nuclei is represented by k_{SD} , and the nuclear spin-lattice relaxation rate is represented by k_{T1} .

nuclei. The reason for this can also be found in spin diffusion that spreads the polarization over a larger volume by means of the nuclear dipolar coupling network. In conventional bulk DNP, spin diffusion is important since

it contributes positively to nuclear polarization buildup. However, under our nanoscale conditions, the polarization pumped from the N-V centers would be rapidly lost out of the sensing volume, so that its accumulation becomes hardly observable with our experiment. In order to rationalize the experimental findings, a simplified kinetic model is setup to describe, at least to a first approximation, the expected buildup of nuclear polarization by continuous repetition of the NOVEL pulse sequence in the presence of simultaneous “loss channels” (see Fig. 5). Here, we consider the transfer of spin polarization to take place together with three interfering processes: electron spin relaxation in the rotating frame ($T_{1\rho}$), nuclear spin-lattice relaxation (T_{1n}), and spin diffusion (T_{SD}). To each of these, specific rate constants are associated. In particular, $k_{SI} = k_{IS}$ are the rates of the polarization transfer from the N-V centers to the nuclei and vice versa and $k_{T1\rho}$ is the rate for the N-V $T_{1\rho}$ relaxation. These have been measured experimentally, as reported above. The nuclear relaxation k_{T1n} and the spin diffusion k_{SD} rates are both estimated based on data reported in the literature [8,16,39] (see Appendix C). Simulations have been performed calculating for each repetition of the sequence the change of the nuclear and electron spin polarizations obtained by the solution of the system of equations reported in Appendix C. In Fig. 6(a), the

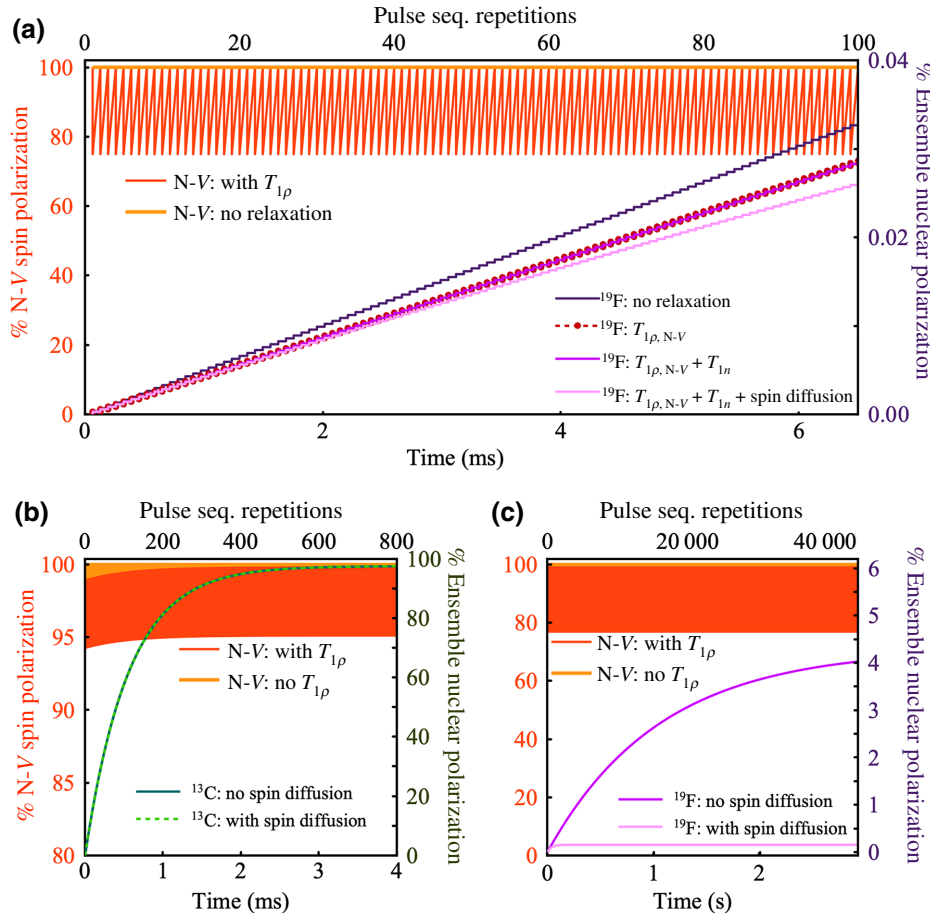


FIG. 6. Simulated polarization buildup curves. Simulation of the N-V and nuclear spin polarizations versus the number of repetitions of the pulse sequence (or the total experimental time) considering the transfer between one N-V center and the nuclear spin ensembles. (a) First 100 repetitions for the transfer from one N-V center to an ensemble of 3000 ^{19}F nuclear spins. Each step corresponds to a $65 \mu\text{s}$ polarization transfer protocol considering the effective rate determined above for this spin ($154 \text{ s}^{-1}/3000$). The red and yellow lines represent electron spin polarization with and without N-V relaxation ($T_{1\rho}$), respectively. The lines from violet to pink show how nuclear buildups are affected by the different “loss channels” considered in the system. (b) Transfer to an ensemble of five ^{13}C spins occurring upon 800 repetitions of the sequence. Steps are $5 \mu\text{s}$ long at the effective rate determined for this spin ($9000 \text{ s}^{-1}/5$). (c) Transfer to the ^{19}F spin bath up to 45 000 repetitions. Both T_{1n} and $T_{1\rho}$ are considered for the nuclear buildups in (b),(c).

simulation of both the N- V and nuclear polarizations during the first 100 repetitions of the pulse sequence is depicted for the case of polarization transfer to a ^{19}F spin ensemble. The N- V polarization is initialized at each repetition, differently from the nuclear polarization that is built up over time. First, it can be noted that the $T_{1\rho}$ relaxation process has a significant effect on the depolarization of the N- V polarization (yellow and red lines) but a rather small effect on the nuclear polarization (violet and dotted magenta line), even at longer timescales. This parameter does not really represent a limit for reaching appreciable polarization buildups. In Fig. 6(b), the buildup curves for ^{13}C are simulated, showing around 800 repetitions of the experiment on a timescale of the order of a few milliseconds to fully polarize the ^{13}C spin bath. In this case both spin diffusion and nuclear spin-lattice relaxation are negligible, since they occur on a timescale much longer than the polarization transfer process. On the contrary, for ^{19}F spins, spin diffusion seems to have a dramatic effect on the polarization buildup, causing the steady-state polarization to decrease by more than an order of magnitude with respect to what is expected when only spin-lattice relaxation is considered [see Fig. 6(c)]. Such a hypothesis appears realistic especially if we think that heteronuclear spin diffusion between ^{19}F and ^1H may also play a role at the low magnetic field at which the experiments are performed. Thus, to accomplish a direct N- V -based detection of enhanced NMR signals, two main approaches can be envisioned: (1) increase the polarization transfer rates; (2) polarization loss pathways need to be circumvented or at least significantly mitigated. About the first point, performing spinlock experiments at higher magnetic fields might be of significant help for the possibility to match the higher nuclear Larmor frequencies with consequently higher spinlock amplitudes. This would advantage the efficiency of the spinlock pulse and of the overall transfer process. Moreover, the use of a resonator for MW delivery instead of the homebuilt MW loop as employed in the present work would significantly reduce the MW field inhomogeneity and greatly improve the performance. Another possible strategy would be to explore alternative polarization transfer schemes that are more robust, in particular for N- V ensembles, and would allow us to improve the transfer rates by more than one order of magnitude [13,40]. However, these schemes are better performed on isotopically enriched ^{12}C diamonds since they can be strongly affected by spurious harmonic signals caused by nearby ^{13}C nuclei [41]. About the second approach, an appropriate engineering of the sample will allow us to conveniently tune the properties of the system so as to decrease diffusion and relaxation. For instance, creating a more “diluted” nuclear spin system with reduced nuclear spin-spin interactions as well as working at higher magnetic fields to inhibit heteronuclear spin diffusion will avoid polarization loss out of the N- V detection volume.

V. CONCLUSION

In summary, we demonstrate spin-polarization transfer between ensembles of shallow N- V centers in diamond and nuclear targets inside and outside the diamond lattice. We find that spinlock pulse sequences based on Hartmann-Hahn matching, such as NOVEL, for the special case of the ensembles have characteristic spectral features. These have to be taken into account and suggest working preferably with higher matching frequencies (i.e., at higher magnetic fields). Furthermore, when performed to address actual nuclear spins, such protocols can lead to significant depletion of N- V spin polarization by HH matching with nuclear spins, even when nuclei are outside the diamond and behind multiple material interfaces. The chemical functionalization of our diamond chip is a well-defined system where several types of nuclear spins could be addressed and their results compared. In the case of nuclei far from the N- V centers, the polarization transfer rates need to be increased to overcome some counteracting processes causing nuclear polarization losses. Apart from nuclear spin relaxation, we identify spin diffusion as the additional process that may hinder a direct N- V -based detection of the transferred polarization. A simplified model based on rate constants has been used to estimate the contribution of spin diffusion to the maximum polarization achievable when typical nuclear spin-lattice relaxation times are considered. This allows us to better define future strategies that can be pursued to achieve the final goal. Based on these results, the implementation of platforms where diamond surface chemistry can be controlled with high accuracy and flexibility prove to be key to establish N- V -based methods for NMR sensitivity enhancement.

All data needed to evaluate the conclusions in the paper are present in the main text and/or in the appendix. Additional data related to this paper may be requested from the authors. All correspondence and requests for materials should be addressed to D.B.B.

ACKNOWLEDGMENTS

This study is funded by the Deutsche Forschungsgemeinschaft (DFG, German Research Foundation) under Grant No. 412351169 within the Emmy Noether program. R.R. acknowledges support from the DFG Walter Benjamin Programme (project RI 3319/1-1). S.G. and D.B.B. acknowledges support from the Deutsche Forschungsgemeinschaft (DFG, German Research Foundation) under Germany’s Excellence Strategy EXC-2111–390814868.

D.B.B. and R.R. conceived the idea; R.R. carried out the experiments, analyzed the data, and performed the simulations; F.B. programmed the pulse sequences; K.S.L. prepared the ALD sample; S.J.G. advised on the theoretical aspects of the work. R.R. wrote the manuscript with input from all authors. All authors reviewed the manuscript and

suggested improvements. D.B.B. supervised the overall research work.

All authors declare that they have no competing interests.

Note added.—Recently, we have become aware of the publication from Healey *et al.* [40], who also demonstrate polarization transfer by means of N-V ensembles in diamond. In relation to this work, our study is different and complementary for the following reasons. (1) The focus of this work is to implement the spinlock experiments for N-V ensembles and understand the spectral features. The polarization transfer in our work relies on using N-V dressed states generated by spinlock pulses, a different approach with respect to Healey *et al.* (Pulsepol). (2) Our chemical system is different, since we address monolayers deposited on the diamond surface and explore the potential of such quasi-two-dimensional structures for nanoscale spin hyperpolarization. (3) Direct polarization transfer has been achieved for ^{19}F nuclei unambiguously positioned outside the diamond lattice and across an additional interface (Al_2O_3 thin film). (4) With this study we propose the use of chemical structures grown on the diamond surface with well-defined characteristics as a testbed for N-V-based spin hyperpolarization at the nanoscale.

APPENDIX A: SIMULATION OF THE SPECTRAL LINESHAPE FOR A SPINLOCK EXPERIMENT

1. Contribution of the off-resonant N-V centers to the linewidth of the N-V depolarization dips

In this section, we derive a formula to predict the contribution of the off-resonant N-V spin packets to the linewidth of the depolarization dips, relative to the rf frequency we aim at matching with the spinlock amplitude. We recall that during the spinlock experiments reported in Fig. 1, the reference rf is set at a constant frequency ν_{rf} and the spinlock MW amplitude ν_{SL} is swept so that matching to the N-V Rabi frequencies $\nu_{\text{IN-V},i} = \sqrt{\Omega_i^2 + \nu_{\text{SL}}^2}$ can occur, where the Ω_i correspond to the offset frequencies of the N-V centers within the ensemble. Thus, for perfectly on-resonance N-V centers ($\Omega_0 = 0$), the spinlock amplitude at which the matching condition is satisfied will simply be $\nu_{\text{SL}} = \nu_{\text{rf}}$, whereas, for off-resonant N-V centers, it will undergo a shift, i.e., $\tilde{\nu}_{\text{SL}} = \sqrt{\nu_{\text{rf}}^2 - \Omega_i^2}$. Such a shift will affect the linewidth of the observed depolarization dip, differently however depending on the rf frequency that is matched. It is possible to calculate such a dependency by using the formula (plotted in Fig. 7)

$$\frac{\nu_{\text{SL}} - \tilde{\nu}_{\text{SL}}}{\nu_{\text{rf}}} = \frac{\nu_{\text{rf}} - \sqrt{\nu_{\text{rf}}^2 - \Omega^2}}{\nu_{\text{rf}}}$$

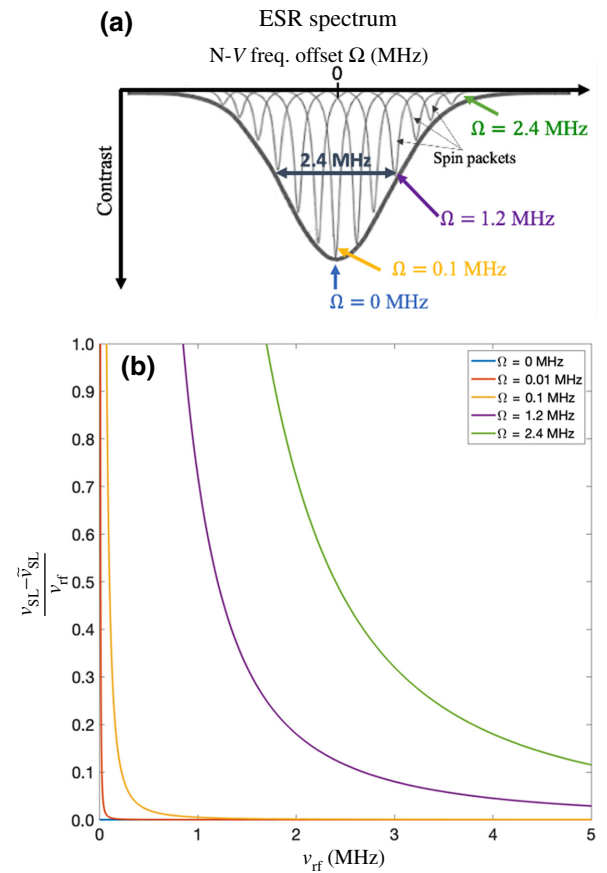


FIG. 7. Contribution of the off-resonant N-V spin packets to the linewidth of the depolarization dip. (a) Schematic representation of the ESR spectrum with the different N-V spin packets resonating at different frequencies within the ESR line. (b) Dependency of the relative spinlock amplitude shift on the rf or Larmor-matched frequency. The dependency is plotted for different detunings from $\Omega = 0$ to 2.4 MHz.

$$\begin{aligned} &= 1 - \sqrt{\frac{\nu_{\text{rf}}^2 - \Omega^2}{\nu_{\text{rf}}^2}} \\ &\approx \frac{1}{2} \left(\frac{\Omega^2}{\nu_{\text{rf}}^2} \right), \end{aligned}$$

since $\sqrt{1-x} \approx 1-x/2$ for small x ($0 \leq x \ll 1$), i.e., for $\Omega \ll \nu_{\text{rf}}$.

2. Simulation of the ensemble spinlock lineshapes

The depolarization peaks reported in Fig. 1(e) are calculated by summing all single contributions (small peaks underneath) corresponding to slightly shifted matching conditions due to off-resonant N-V centers (“spin packets” having different ESR resonance offset Ω_i). A MATLAB[®] script is coded to perform the calculation according to the following scheme: for each Ω_i within the ESR line

(see Fig. 7), a weighting factor L is calculated corresponding to a normalized Lorentzian intensity having the same linewidth (LW) as the experimental ESR line; see Fig. 1(c). Then, $L_i = 1/(1 + x^2)$, where $x = \Omega_i/(LW/2)$ and $LW = 2.4$ MHz. Such a factor is then multiplied by the i th depolarization dip dip_i , again utilizing a Lorentzian function as $dip_i = -[1/(1 + x_{dip}^2)]L_i$, where $x_{dip} = (\nu_{SL} - |\tilde{\nu}_{SL}|)/(LW_{dip}/2)$ and $LW_{dip} = 60$ kHz is fit to best reproduce the line broadening observed in the experiments. The lineshape of the depolarization dips by the PROPI experiment reported in Fig. 3(e) are also simulated following the same approach for the matched ^1H (light blue dips) and ^{19}F (dark blue dips) cases. In the figure, the intensity of the small dips corresponding to single off-resonant contributions is multiplied by a factor of 3 only for a better visualization.

APPENDIX B: RAW DATA

In this section the raw data for the N- V depolarization detection by PROPI and NOVEL experiments are reported. As visible in Figs. 8–10 such experiments show a typical baseline where the overall contrast increases with the spinlock amplitude. This is due to the fact that, after the strong excitation of the N- V spins by the first $\pi/2$ pulse, the spinlock amplitude is stepwise increased and the stronger the spinlock pulse becomes, the more efficiently it is able to lock the N- V spins on the transverse plane. In Fig. 1, the baseline removal is accomplished by subtracting a dataset of the same experiment performed with no rf signal. In Figs. 3(c) and 3(d) the baseline is removed by subtracting a polynomial function fitting to the data of the spectral ranges that contain no peaks. In the following experiments shown, the spinlock amplitude is reported in units of peak-to-peak voltage (V p.p.) as directly read out from our AWG.

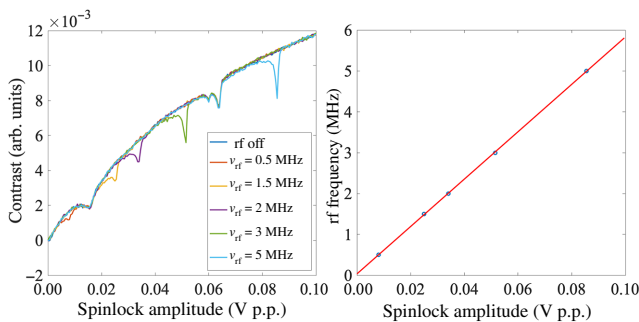


FIG. 8. Calibration of the spinlock experiment by means of an external rf signal. Left: the signal is acquired by averaging each point 5000 times and the whole sweep repeated 3 times. Right: the spinlock amplitudes at which the depolarization dips appeared upon application of the different ν_{rf} are read out and plotted. A linear fit is shown in red.

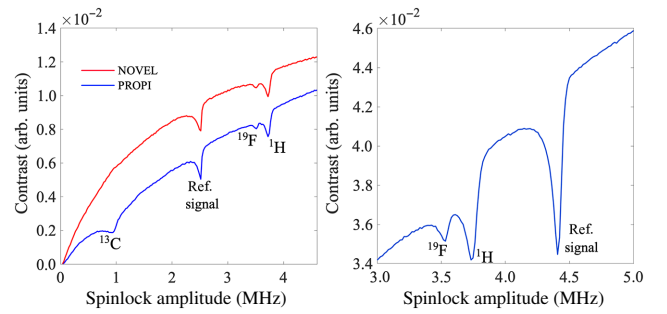


FIG. 9. Raw data for the SAM layer on the diamond. Left: 5000 averages for 20 sweeps. Right: 5000 averages for 250 sweeps.

1. Optimization of the driving MW field

The ESR frequency measured from the dip in PL [see Fig. 1(c)] is used to determine the magnetic field strength and the N- V resonance frequency to perform a Rabi experiment, which then determines the $\pi/2$ pulse duration for the spinlock sequences. A thorough optimization of the MW delivery is of crucial importance for the spinlock experiment to be successful and is mainly accomplished by finding the conditions that minimize the damping of the Rabi oscillations. This indicates that the MW field across the N- V ensemble is homogeneous enough to achieve an efficient spinlock (Fig. 11).

2. Fittings of the dynamics data

Each dataset in Figs. 4(a), 4(c), and 4(e) is normalized to the contrast detected after a strong π pulse. The depicted decays start from only a fraction of the available N- V polarization because of a fast polarization loss during the first few microseconds of the spinlock time (not shown). Such a behavior is likely due to the low MW amplitude of the driving field that causes inefficient spin locking and consequent fast N- V $T_{1\rho}$ relaxation. The data points for “unmatched HH” in Figs. 4(a), 4(c), and 4(e) are fit with a double exponential function whose slower components are chosen to

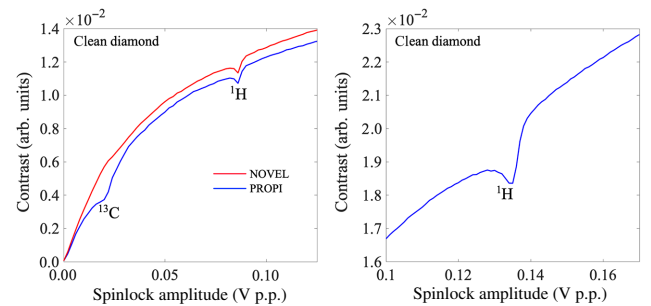


FIG. 10. Raw data for the clean diamond. Signal acquisition: 5000 averages for 20 sweeps.

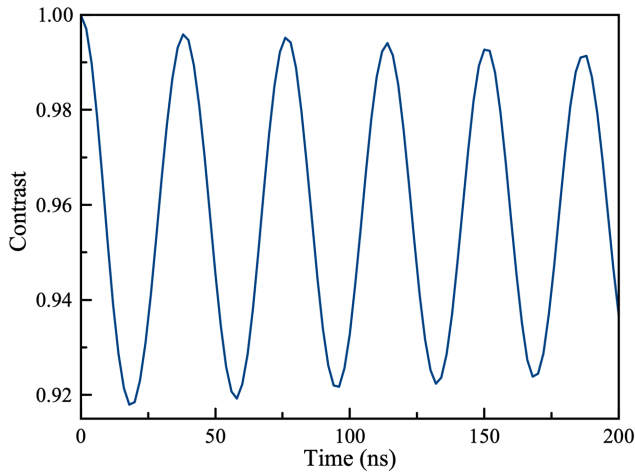


FIG. 11. A typical Rabi experiment with N- V ensembles. The typical contrast of the Rabi oscillations is around 7%–8%. This experiment allows us to calibrate the pulse length but to also optimize the homogeneity of the MW field throughout the N- V ensemble.

represent the N- V relaxation rate constants $k_{T_{1\rho}}$. In particular, for ^1H and ^{19}F , $k_{T_{1\rho}} \approx 4500 \text{ s}^{-1}$, whereas for ^{13}C , $k_{T_{1\rho}} \approx 9200 \text{ s}^{-1}$. In order to maintain constant experimental conditions for comparison, the unmatched HH decay curves had to be acquired at a slightly shifted spinlock amplitude (next to the matching point). This causes an overestimation of the polarization transfer rates by 3%, 8%, and 25%, respectively, for ^{13}C , ^1H , and ^{19}F .

APPENDIX C: SIMULATION OF POLARIZATION BUILDUPS

All polarization curves reported in Fig. 6 are simulated by implementing in a MATLAB code the model schematically depicted in Fig. 5. In particular, the code solves the system of ordinary differential equations

$$\begin{aligned} \frac{dP_S}{dt} &= -k_{SI}P_S + k_{IS}P_I - k_{T_{1\rho}}P_S, \\ \frac{dP_I}{dt} &= -k_{IS}P_I + k_{SI}P_S - k_{T_{1n}}P_I - k_{T_{SD}}P_I, \end{aligned}$$

for a time duration dictated by the optimal spinlock time that is experimentally determined (e.g., $65 \mu\text{s}$ for ^{19}F or $5 \mu\text{s}$ for ^{13}C). Then, depending on the number of pulse sequence repetitions that we want to simulate, the code is looped, resetting only the electron spin polarization $P_S = 1$ each time. Rate constants, where possible, are measured with the experiments reported above. The nuclear spin-lattice relaxation T_{1n} is considered to be of the order of 100 s for ^{13}C inside the diamond and 1 s for both ^1H and ^{19}F [8,39]. The spin diffusion time constant T_{SD} is derived using a formula adopted from simple random walk theory $T_{SD} \approx r^2/(4D)$, where r is the average displacement and

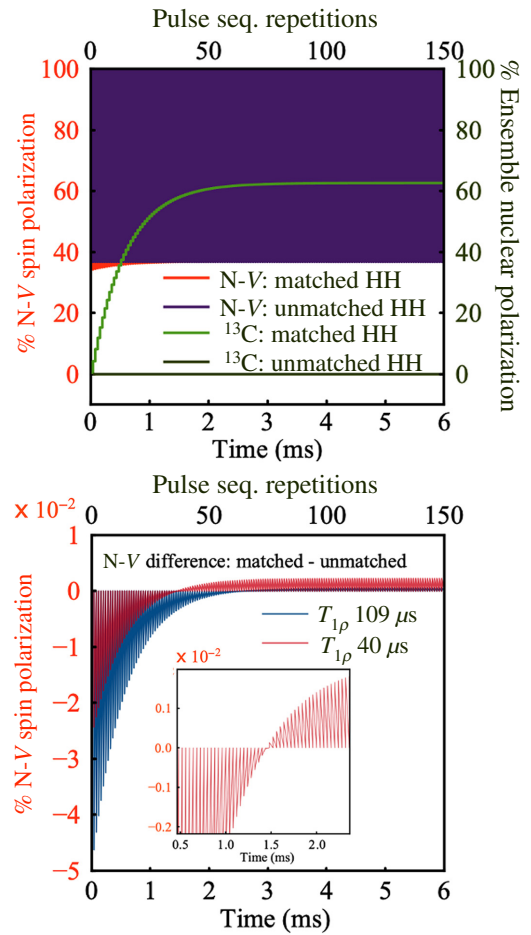


FIG. 12. Inversion of the depolarization dip at ^{13}C matching observed during NOVEL. (a) Simulation of the N- V (red) and nuclear (green) spin polarizations as a function of the pulse sequence repetitions for the cases when (i) the polarization transfer rates are activated (matched HH) and (ii) the polarization transfer rates are off (unmatched). Spinlock pulse duration is $40 \mu\text{s}$, with all other rates as in Fig. 6. (b) Difference between the calculated N- V polarization for the cases when the HH condition is matched and unmatched. The decay at the first pulse sequence corresponds to the full intensity of the depolarization dip (the same observed during a PROPI experiment). After some repetitions of the pulse sequence, the dip gets less and less intense until it inverts. The simulation is shown for two different $T_{1\rho}$ time constants (red, $40 \mu\text{s}$; blue, $109 \mu\text{s}$).

D is the spin diffusion constant. This gives an estimation of how long it takes for the polarization generated in one point of the sensing area to leave the detection volume of the N- V center. Here we consider $D = 700 \text{ nm}^2 \text{ s}^{-1}$ and $r = 10 \text{ nm}$ for both ^{19}F and ^1H , and $D = 0.0035 \text{ nm}^2 \text{ s}^{-1}$ ([16]) and $r = 1 \text{ nm}$ for ^{13}C . The inverted depolarization dip observed for ^{13}C during the NOVEL experiment and reported in Fig. 3 can also be rationalized by means of our simplified rate equations model. In the same manner as done for Fig. 6, in Fig. 12 the percentage of N- V spin

polarization is reported versus the number of pulse sequence repetitions. At the start of each pulse sequence, the N- V spin is reset to 100% polarization, whereas the nuclear spin polarization is allowed to build up during a 40 μ s spinlock time (the same pulse length used in the experiment of Fig. 3). We note that, due to the decay of the N- V polarization caused by the $T_{1\rho}$ relaxation, at a certain point of the dynamics the nuclear spin bath reaches a polarization higher than that of the N- V spins. Thus, after reaching this point and for the subsequent repetitions, the spinlock pulse can partially work in the opposite direction, letting some polarization flow back from the nuclear to the N- V spins. This will occur during the last fraction of the spinlock duration, that is, after the N- V ensemble is relaxed to a polarization level lower than the nuclear one. When we compare the signal for the matched HH condition with that where no condition is met (as we do experimentally when we compare the intensity of the dip to the baseline), we see that the mechanism described above results in an inversion of the “depolarization dip” and this effect can become more severe the shorter the $T_{1\rho}$ time constant and/or the longer the spinlock time.

-
- [1] A. W. Overhauser, Polarization of nuclei in metals, *Phys. Rev.* **92**, 411 (1953).
- [2] S. J. Nelson *et al.*, Metabolic imaging of patients with prostate cancer using hyperpolarized [1- 13 C]Pyruvate, *Sci. Transl. Med.* **5**, 198 (2013).
- [3] J.-H. Ardenkjaer-Larsen, G. S. Boebinger, A. Comment, S. Duckett, A. S. Edison, F. Engelke, C. Griesinger, R. G. Griffin, C. Hilty, H. Maeda, G. Parigi, T. Prisner, E. Ravera, J. van Bentum, S. Vega, A. Webb, C. Luchinat, H. Schwalbe, and L. Frydman, Facing and overcoming sensitivity challenges in biomolecular NMR spectroscopy, *Angew. Chem. Int. Ed.* **54**, 9162 (2015).
- [4] A. S. Lilly Thankamony, J. J. Wittmann, M. Kaushik, and B. Corzilius, Dynamic nuclear polarization for sensitivity enhancement in modern solid-state NMR, *Prog. Nucl. Magn. Reson. Spectrosc.* **102**, 120 (2017).
- [5] J. R. Maze, P. L. Stanwix, J. S. Hodges, S. Hong, J. M. Taylor, P. Cappellaro, L. Jiang, M. V. G. Dutt, E. Togan, A. S. Zibrov, A. Yacoby, R. L. Walsworth, and M. D. Lukin, Nanoscale magnetic sensing with an individual electronic spin in diamond, *Nature* **455**, 644 (2008).
- [6] G. Balasubramanian, I. Y. Chan, R. Kolesov, M. Al-Hmoud, J. Tisler, C. Shin, C. Kim, A. Wojcik, P. R. Hemmer, A. Krueger, T. Hanke, A. Leitenstorfer, R. Bratschkitsch, F. Jelezko, and J. Wrachtrup, Nanoscale imaging magnetometry with diamond spins under ambient conditions, *Nature* **455**, 648 (2008).
- [7] C. Belthangady, N. Bar-Gill, L. M. Pham, K. Arai, D. Le Sage, P. Cappellaro, and R. L. Walsworth, Dressed-State Resonant Coupling between Bright and Dark Spins in Diamond, *Phys. Rev. Lett.* **110**, 157601 (2013).
- [8] J.-P. Tetienne, L. T. Hall, A. J. Healey, G. A. L. White, M.-A. Sani, F. Separovic, and L. C. L. Hollenberg, Prospects for nuclear spin hyperpolarization of molecular samples using nitrogen-vacancy centers in diamond, *Phys. Rev. B* **103**, 014434 (2021).
- [9] J. P. King, P. J. Coles, and J. A. Reimer, Optical polarization of 13 C nuclei in diamond through nitrogen vacancy centers, *Phys. Rev. B* **81**, 073201 (2010).
- [10] P. London, J. Scheuer, J.-M. Cai, I. Schwarz, A. Retzker, M. B. Plenio, M. Katagiri, T. Teraji, S. Koizumi, J. Isoya, R. Fischer, L. P. McGuinness, B. Naydenov, and F. Jelezko, Detecting and Polarizing Nuclear Spins with Double Resonance on a Single Electron Spin, *Phys. Rev. Lett.* **111**, 067601 (2013).
- [11] D. Pagliero, K. R. K. Rao, P. R. Zangara, S. Dhomkar, H. H. Wong, A. Abril, N. Aslam, A. Parker, J. King, C. E. Avalos, A. Ajoy, J. Wrachtrup, A. Pines, and C. A. Meriles, Multispin-assisted optical pumping of bulk 13 C nuclear spin polarization in diamond, *Phys. Rev. B* **97**, 024422 (2018).
- [12] A. Ajoy, K. Liu, R. Nazaryan, X. Lv, P. R. Zangara, B. Savvati, G. Wang, D. Arnold, G. Li, A. Lin, P. Raghavan, E. Druga, S. Dhomkar, D. Pagliero, J. A. Reimer, D. Suter, C. A. Meriles, and A. Pines, Orientation-independent room temperature optical 13 C hyperpolarization in powdered diamond, *Sci. Adv.* **4**, eaar5492 (2018).
- [13] I. Schwartz, J. Scheuer, B. Tratzmiller, S. Müller, Q. Chen, I. Dhand, Z.-Y. Wang, C. Müller, B. Naydenov, F. Jelezko, and M. B. Plenio, Robust optical polarization of nuclear spin baths using Hamiltonian engineering of nitrogen-vacancy center quantum dynamics, *Sci. Adv.* **4**, eaat8978 (2018).
- [14] P. Fernández-Acebal, O. Rosolio, J. Scheuer, C. Müller, S. Müller, S. Schmitt, L. McGuinness, I. Schwarz, Q. Chen, A. Retzker, B. Naydenov, F. Jelezko, and M. Plenio, Toward hyperpolarization of oil molecules via single nitrogen vacancy centers in diamond, *Nano Lett.* **18**, 1882 (2018).
- [15] F. Shagieva, S. Zaiser, P. Neumann, D. B. R. Dasari, R. Stöhr, A. Denisenko, R. Reuter, C. A. Meriles, and J. Wrachtrup, Microwave-assisted cross-polarization of nuclear spin ensembles from optically pumped nitrogen-vacancy centers in diamond, *Nano Lett.* **18**, 3731 (2018).
- [16] D. A. Broadway, J.-P. Tetienne, A. Stacey, J. D. A. Wood, D. A. Simpson, L. T. Hall, and L. C. L. Hollenberg, Quantum probe hyperpolarisation of molecular nuclear spins, *Nat. Commun.* **9**, 1246 (2018).
- [17] D. R. Glenn, D. B. Bucher, J. Lee, M. D. Lukin, H. Park, and R. L. Walsworth, High-resolution magnetic resonance spectroscopy using a solid-state spin sensor, *Nature* **555**, 351 (2018).
- [18] J. Smits, J. T. Damron, P. Kehayias, A. F. McDowell, N. Mosavian, I. Fescenko, N. Ristoff, A. Laraoui, A. Jarmola, and V. M. Acosta, Two-dimensional nuclear magnetic resonance spectroscopy with a microfluidic diamond quantum sensor, *Sci. Adv.* **5**, eaaw7895 (2019).
- [19] D. B. Bucher, D. R. Glenn, H. Park, M. D. Lukin, and R. L. Walsworth, Hyperpolarization-Enhanced NMR Spectroscopy with Femtomole Sensitivity Using Quantum Defects in Diamond, *Phys. Rev. X* **10**, 021053 (2020).

- [20] N. Arunkumar, D. B. Bucher, M. J. Turner, P. TomHon, D. Glenn, S. Lehmkuhl, M. D. Lukin, H. Park, M. S. Rosen, T. Theis, and R. L. Walsworth, Micron-scale NV-NMR spectroscopy with signal amplification by reversible exchange, *PRX Quantum* **2**, 010305 (2021).
- [21] K. S. Liu, A. Henning, M. W. Heindl, R. D. Allert, J. D. Bartl, I. D. Sharp, R. Rizzato, and D. B. Bucher, Surface NMR using quantum sensors in diamond, *Proc. Natl. Acad. Sci.* **119**, e2111607119 (2022).
- [22] A. Henstra, P. Dirksen, J. Schmidt, and W. Wenckebach, Nuclear spin orientation via electron spin locking (NOVEL), *J. Magn. Reson.* **77**, 389 (1988).
- [23] H. Brunner, R. H. Fritsch, and K. H. Hausser, Notizen: Cross polarization in electron nuclear double resonance by satisfying the hartmann-hahn condition, *Zeitschrift für Naturforschung A* **42**, 1456 (1987).
- [24] J. Scheuer and B. Naydenov, Dynamic nuclear polarization (DNP) in diamond, semiconductors and semimetals, Elsevier, *Semicond. Semimetals* **103**, 277 (2020).
- [25] S. R. Hartmann and E. L. Hahn, Nuclear double resonance in the rotating frame, *Phys. Rev.* **128**, 2042 (1962).
- [26] V. Weis and R. Griffin, Electron-nuclear cross polarization, *Solid State Nucl. Magn. Reson.* **29**, 66 (2006).
- [27] R. Rizzato and M. Bennati, Cross-polarization electron-nuclear double resonance spectroscopy, *ChemPhysChem* **16**, 3769 (2015).
- [28] J. Scheuer, I. Schwartz, S. Müller, Q. Chen, I. Dhand, M. B. Plenio, B. Naydenov, and F. Jelezko, Robust techniques for polarization and detection of nuclear spin ensembles, *Phys. Rev. B* **96**, 174436 (2017).
- [29] F. Shagieva, NMR spectroscopy with single shallow NV centers, 10.18419/OPUS-10528, Universität Stuttgart (2019).
- [30] D. B. Bucher, D. P. L. Aude Craik, M. P. Backlund, M. J. Turner, O. Ben Dor, D. R. Glenn, and R. L. Walsworth, Quantum diamond spectrometer for nanoscale NMR and ESR spectroscopy, *Nat. Protoc.* **14**, 2707 (2019).
- [31] F. Ziem, M. Garsi, H. Fedder, and J. Wrachtrup, Quantitative nanoscale MRI with a wide field of view, *Sci. Rep.* **9**, 12166 (2019).
- [32] S. J. DeVience, L. M. Pham, I. Lovchinsky, A. O. Sushkov, N. Bar-Gill, C. Belthangady, F. Casola, M. Corbett, H. Zhang, M. Lukin, H. Park, A. Yacoby, and R. L. Walsworth, Nanoscale NMR spectroscopy and imaging of multiple nuclear species, *Nat. Nanotechnol.* **10**, 129 (2015).
- [33] K. J. Brown, E. Chartier, E. M. Sweet, D. A. Hopper, and L. C. Bassett, Cleaning diamond surfaces using boiling acid treatment in a standard laboratory chemical hood, *J. Chem. Health Safety* **26**, 40 (2019).
- [34] T. Staudacher, N. Raatz, S. Pezzagna, J. Meijer, F. Reinhard, C. A. Meriles, and J. Wrachtrup, Probing molecular dynamics at the nanoscale via an individual paramagnetic centre, *Nat. Commun.* **6**, 8527 (2015).
- [35] S. Felton, A. M. Edmonds, M. E. Newton, P. M. Martineau, D. Fisher, D. J. Twitchen, and J. M. Baker, Hyperfine interaction in the ground state of the negatively charged nitrogen vacancy center in diamond, *Phys. Rev. B* **79**, 075203 (2009).
- [36] B. Smeltzer, L. Childress, and A. Gali, ^{13}C hyperfine interactions in the nitrogen-vacancy centre in diamond, *New J. Phys.* **13**, 025021 (2011).
- [37] A. Dréau, J.-R. Maze, M. Lesik, J.-F. Roch, and V. Jacques, High-resolution spectroscopy of single NV defects coupled with nearby ^{13}C nuclear spins in diamond, *Phys. Rev. B* **85**, 134107 (2012).
- [38] G. A. Álvarez, C. O. Bretschneider, R. Fischer, P. London, H. Kanda, S. Onoda, J. Isoya, D. Gershoni, and L. Frydman, Local and bulk ^{13}C hyperpolarization in nitrogen-vacancy-centred diamonds at variable fields and orientations, *Nat. Commun.* **6**, 8456 (2015).
- [39] A. Ajoy, B. Safvati, R. Nazaryan, J. T. Oon, B. Han, P. Raghavan, R. Nirodi, A. Aguilar, K. Liu, X. Cai, X. Lv, E. Druga, C. Ramanathan, J. A. Reimer, C. A. Meriles, D. Suter, and A. Pines, Hyperpolarized relaxometry based nuclear T_1 noise spectroscopy in diamond, *Nat. Commun.* **10**, 5160 (2019).
- [40] A. Healey, L. Hall, G. White, T. Teraji, M.-A. Sani, F. Separovic, J.-P. Tetienne, and L. Hollenberg, Polarization Transfer to External Nuclear Spins Using Ensembles of Nitrogen-Vacancy Centers, *Phys. Rev. Appl.* **15**, 054052 (2021).
- [41] M. Loretz, J. M. Boss, T. Roskopf, H. J. Mamin, D. Rugar, and C. L. Degen, Spurious Harmonic Response of Multipulse Quantum Sensing Sequences, *Phys. Rev. X* **5**, 021009 (2015).